Journal of Materials Chemistry C

Elastic broadband antireflection coatings for flexible optics using multi-layered polymer thin films

Journal:	*Journal of Materials Chemistry C*
Manuscript ID	TC-ART-01-2023-000104.R1
Article Type:	Paper
Date Submitted by the Author:	14-Feb-2023
Complete List of Authors:	Zhao, Yineng; University of Rochester, Materials Science Huo, Ni; University of Rochester, Chemical Engineering Ye, Sheng; Meta Reality Labs Tenhaeff, Wyatt; University of Rochester, Chemical Engineering

ARTICLE

Elastic broadband antireflection coatings for flexible optics using multi-layered polymer thin films

Received 00th January 20xx,
Accepted 00th January 20xx

DOI: 10.1039/x0xx00000x

Yineng Zhao,[a] Ni Huo,[b] Sheng Ye,[c] and Wyatt E. Tenhaeff *[a, b]

Flexible optics and optoelectronic devices require stretchable and compliant antireflection coatings (ARC). Conventional optical coatings, typically inorganic thin films, are brittle and crack under strain, while porous or patterned surfaces often lack environmental endurance and/or involve complex processing. Polymeric optical thin films prepared by initiated chemical vapor deposition (iCVD) comprise a promising alternative class of materials. With iCVD, multilayered, uniform thin film coatings can be synthesized conformally on the surface of a temperature-sensitive substrate near room temperature with precise compositional and thickness control. In this study, a model two-layer coating design consisting of poly(1H,1H,6H,6H-perfluorohexyl diacrylate) (pPFHDA) with a refractive index at 633 nm of n_{633}=1.426 was deposited atop poly(4-vinylpyridine) (p4VP, n_{633}=1.587). Broadband antireflection over the visible wavelength range (400-750 nm) was conferred to a transparent, flexible thermoplastic polyurethane (TPU) substrate (n_{633}~1.51), reducing the front-surface reflectance from ~4% to ~2%. The superior mechanical compliance of polymer ARCs over conventional inorganic coatings (MgF_2, SiO_2, and Al_2O_3) on the TPU substrate was thoroughly investigated by monitoring the evolution of film morphology and tensile fracture with applied equibiaxial strain. The polymer ARC withstood at least ε=1.64% equibiaxial strain without fracture, while all inorganic coatings cracked. Through a repeated application of strain over hundreds of cycles, the antireflection by the polymer film was shown to possess excellent stability and fatigue resilience. Finally, simulations of established iCVD polymer chemistries possessing larger index contrast revealed that reflectance can be further reduced to <1% or better.

Introduction

Antireflection coatings (ARCs) are essential components in modern high-performance optical and optoelectronic devices. They reduce the reflection of light at the interface between the optical material and its medium, minimize undesired lens flare and glare, and increase transmission. Antireflection coatings typically consist of single or multiple thin film coatings with precisely engineered optical thicknesses, such that reflected light at the layer interfaces interferes destructively to minimize reflectance.[1-4] Practical broadband antireflection coating designs require thin film materials that 1) are transparent in the desired wavelength range (minimal absorption and scattering); 2) offer a wide range of accessible refractive index; 3) can be created with high thickness precision; 4) possess good mechanical properties, such as scratch resistance and adhesion to the substrate; and 5) are chemically and physically stable in the targeted environment.

Conventional antireflection coatings are dominated by inorganic compounds, such as MgF_2, Al_2O_3, SiO_2, and TiO_2.[1, 4-6] Inorganic fluorides, oxides, and sulfides offer excellent transparency over a broad wavelength range, from near-UV to near-IR, and a wide range of accessible refractive indexes. Among dense films, MgF_2 possesses one of the lowest refractive indexes (~1.38). It is widely used as a single-layer ARC for common glass (index ~1.51; ideal index of its single-layer ARC is ~1.23), as well as the low index component in multilayer ARCs.[1] TiO_2 has a reported index of 2.56, providing an index contrast of 1.18 relative to MgF_2, which is oft exploited in ARC designs.[7-10] Moreover, these materials are stable in the air over wide ranges of temperature and humidity. In fact, some of these layers find application as transparent barrier layers, replacing opaque metallic thin films.[11-13] Given the importance of these inorganic thin films, a multitude of vacuum deposition techniques based on either physical vapor deposition or chemical vapor deposition have been developed, providing high throughput fabrication of precisely controlled optical layer designs.[10, 14]

However, the brittleness of inorganic-based ARCs is a significant limitation when applied to flexible, elastomeric substrates, which are being explored for next-generation optical systems. As optical and optoelectronic devices are becoming increasingly compact, flexible, and adaptive in recent years–the development of wearable displays, adaptive augmented reality/virtual reality hardware, and flexible photovoltaics are a few examples–there is a critical need for

[a] Materials Science Program, University of Rochester, Rochester, New York 14627, United States
[b] Department of Chemical Engineering, University of Rochester, Rochester, New York 14627, United States
[c] Meta Reality Labs, 9845 Willows Rd, Redmond, Washington 98052, United States
Yineng Zhao and Ni Huo contributed equal effort to this work.
Electronic Supplementary Information (ESI) available: [details of any supplementary information available should be included here]. See DOI: 10.1039/x0xx00000x

ARCs that can be incorporated with flexible substrates.[15-19] The mismatch in elastic properties and coefficients of thermal expansion between the optical layers and polymeric substrate results in fracture (cracking) and/or film delamination with slight strain or temperature excursions.[18] Even minute moisture absorption can lead to volumetric stresses that result in coating failure.[20] Another practical challenge can arise due to the heat flux on the polymer substrate during vacuum deposition, which can lead to undesirable morphological changes in the polymeric substrate and/or residual film stresses.[21, 22]

On the other hand, polymer thin film coatings possessing elastic properties and thermal expansivities that are comparable to the underlying substrate are expected to be better suited for flexible optics, yet an important limitation is their limited range of refractive indexes. Conventional thermoplastics have refractive indexes that fall into a relatively small range - approximately between 1.35 to 1.70.[23] This index contrast of 0.35 is markedly smaller than that can be achieved with established inorganic coatings.[24, 25] To compensate for this limited index contrast, a common design strategy is to increase the number of layers in the multilayer coating to give a higher degree of freedom in manipulating interference so more significant antireflection over a larger bandwidth can be achieved.[26] However, the fabrication of multiple polymer layers with nanometer-level precision in thickness is a challenge for conventional solution processing of polymers. Wet coating techniques, such as spin coating and dip coating, typically require sequential application of polymers from solutions. However, the solvents can also cause swelling and even dissolution of the previously coated layers.[27-29] Although careful selection of polymer combinations with orthogonal solubilities can mitigate these problems at the expense of design freedom, solvent penetration into the multilayer structure can still damage buried layers and lead to deleterious film stresses that compromise the coating.[29-33] Another mature technique, melt polymer coextrusion, can successfully fabricate a large number of polymer multilayers at a large scale with thickness down to tens of nanometers of each layer.[34-36] However, the film stacks usually consist of layers with repeated thickness combinations; the thicknesses of an individual layer cannot be independently tuned. Moreover, its thickness control is highly dependent on precise control of the laminar flow of melt polymers and a thorough understanding of the rheological behavior of each polymer during the coextrusion.[37] Both solution processing and coextrusion techniques lack the key ability to *in situ* monitor nascent film thickness during fabrication, which complicates reproducible thickness control and tuning. Vacuum deposition techniques, on the other hand, enable *in situ* monitoring of layer thicknesses during sequential multilayer deposition. Only a select few polymers can be deposited by physical vapor deposition, such as sputtering, pulsed laser, or thermal evaporation, and the process often leads to chain fragmentation and other compositional defects.[38-44] Molecular layer deposition (MLD) and conventional CVD offer greater control over film chemistries, but often require elevated temperatures, making integration with temperature-sensitive thermoplastic substrates difficult.[45, 46] Finally, plasma-enhanced CVD (PECVD) is a well-established technique, but the energetic plasma generates a distribution of highly reactive intermediates resulting in undefined chemical composition and possibly light absorption.[27, 46] Another promising approach alternative to coatings is to engineer antireflection through surface patterns or porous structures directly applied to the flexible substrate, but their complex multi-step fabrication processes and limited mechanical durability currently limit their practical implementation.[2, 47-51]

In this work, initiated chemical vapor deposition (iCVD) was introduced to deposit a model two-layer polymeric interference antireflection coating on an aliphatic thermoplastic polyurethane (TPU) elastomeric substrate with a precisely designed structure. The optical-grade TPU was chosen as the substrate in this work because of its high transparency and excellent mechanical flexibility, suitable for flexible optics. It was also used as the substrate in our previous study of developing a barrier layer for flexible optics.[52] The two polymer layers were poly(1H, 1H, 6H, 6H-perfluorohexyl diacrylate) (pPFHDA) and poly(4-vinyl pyridine) (p4VP), which have distinct refractive indexes of 1.43 and 1.59, respectively (measured at 633 nm). iCVD is an established vacuum deposition technique capable of conformally synthesizing uniform polymer thin films *in situ* on a substrate surface near room temperatures, which is critical to avoid unwanted phase transformations and/or thermal stresses in the substrate.[46, 53-55] The solvent-free nature of the technique is especially critical as it spares the multilayered systems from the complications associated with swelling or dissolution as discussed above. Moreover, through precise control of the process chemistry, polymer film compositions can be carefully engineered to tune optical properties, and crosslinking can be incorporated as needed to modulate mechanical properties.[56] It was reported in our previous work that the highly crosslinked pPFHDA used in this work as the top layer also functions as a highly effective barrier layer.[52]

We demonstrate for the first time the preparation of a fully polymeric model two-layer antireflection coating by iCVD and explore the mechanical compliance relative to other conventional inorganic optical layers through direct in situ evaluation of coating failure as a function of applied equibiaxial strain. The work builds upon previous studies where pPFHDA-based barrier layers were deposited onto flexible TPU substrates with excellent compositional fidelity, thickness uniformity, and adhesion.[52] Several conventional coating materials (MgF_2, SiO_2, Al_2O_3) and thicknesses were also explored to understand the generality of film fracture of inorganic coatings on elastomeric substrates. Subsequently, cracks were deliberately generated in the polymer coating through cyclic application of aggressive strain to monitor their evolution over time and impact on antireflection performance.

Experimental Section

Film synthesis

A custom-built vacuum system was used to execute initiated chemical vapor deposition (iCVD). A 35×30×10 cm stainless steel reaction chamber was connected to a rotary vane vacuum pump. The pressure in the reaction chamber was monitored and controlled by a pressure gauge (Brooks, XacTorr CMX100) and a downstream throttle control valve (MKS 653B) connected by a digital pressure controller (MKS 600 Series). A hot filament array (Master Wire, Nichrome 80) was fixed 2.5 cm above a temperature-controlled stage (~16×15×2 cm) with a power of 46.5±0.4 W (0.7 A × 66.4 ±0.6 V) provided by a DC power supply (TDK Lambda, GEN 150-5-USB-U). The temperature stage (aluminum base, copper surface) (Wieland MicroCool) was back-chilled by a recirculation chiller/heater (VWR, AD07R-20) to maintain a constant substrate temperature. Flows of carrier gas (MKS, Type 1179), diluent gas (MKS, Type 1479A), and initiator (Horiba STEC, SEC-4400) were regulated by mass flow controllers. Argon (Airgas, high purity grade) was used as the carrier and diluent gas.

Transparent aliphatic thermoplastic polyurethane (TPU) membranes were provided by Sheedom Co. TPU was stretched and fixed to a round stainless-steel ring using a Schmidt ring press. The back side of the ring was embedded with an O-ring to ensure gas-sealing so the membrane can be deformed pneumatically. The TPU membrane was 7.7 cm in diameter with a thickness measured to be about 230 μm by a micrometer. During the deposition, the TPU membrane was placed on a copper base, making solid contact between the temperature-controlled stage and the substrate to ensure thermal transport. The temperature stage was kept at 35°C. 1H,1H,6H,6H-perfluorohexyl diacrylate (PFHDA, SynQuest Laboratories, 99% purity) and 4-vinylpyridine (4VP, ACROS, 97% purity) were kept in monomer jars immersed in a 25°C water bath (Cole-Parmer, StableTemp WB05). Di-tert-butyl peroxide initiator (TBPO, Acros Organics, 99% purity) vapor flow rate was fixed at 2 sccm. The p4VP was deposited on the TPU first, with a carrier gas flow at 5 sccm and diluent gas at 10 sccm. The deposition rate was around 1.7 nm/min. The thickness was in situ monitored by laser interferometry. After the target thickness of p4VP was reached, the flow of 4VP was stopped and the chamber was pumped down to base pressure with 100 sccm pure argon purging for 1 min. Shortly, the carrier gas of PFHDA was turned on at a flow rate of 50 sccm and the diluent gas flowed at 100 sccm to coat the second layer–pPFHDA. The deposition rate of pPFHDA was about 1.0 nm/min. The chamber pressure was kept at 750 mTorr during the deposition of both polymers.

Inorganic coatings, MgF_2, SiO_2, and Al_2O_3, were all prepared by electron beam deposition (e-beam) in a Kurt J. Lesker PVD-75 deposition chamber. The deposition target materials were placed in a graphite crucible, and the TPU sample was fastened to the substrate holder above the target. The chamber was pumped down to 5×10^{-6} Torr before each deposition. The e-beam currents for MgF_2, SiO_2, and Al_2O_3 were about 0.5 mA, 12 mA, and 50 mA, respectively; a slow deposition rate of around 0.5 Å/s was maintained aiming to achieve a low-stress high-quality optical-grade film. 1.5 sccm O_2 and 0.75 sccm Ar were introduced to create an oxidizing environment for SiO_2 and Al_2O_3 depositions to compensate for possible oxygen loss and maintain the correct stoichiometry. The chamber pressure during e-beam depositions is around 5×10^{-5} Torr for MgF_2 and $2.5\text{-}3.5\times10^{-4}$ Torr for the oxides. The thickness of the inorganic coatings was monitored by a quartz crystal microbalance (QCM) inside the chamber during the deposition and also characterized by ellipsometry directly on TPU after the deposition.

Material characterizations

Fourier transform infrared spectroscopy (FTIR) was conducted on Thermo Fisher Scientific Nicolet iS50. The spectra of TPU coated with the p4VP and pPFHDA double layer, the uncoated TPU, pure p4VP, pure pPFDA, pure 4VP, and pure PFHDA monomers were all characterized by attenuated total reflectance (ATR, Specac GoldenGate) with the ATR correction applied. The pure polymers of p4VP and pPFHDA were scratched from a monolayer coating deposited on a Si wafer under the same condition as the two-layer deposition on TPU. For all measurements, the resolution was set to 4 cm^{-1} and a total of 64 scans were integrated to improve the signal-to-noise ratio of the spectra.

The optical constants and the film thicknesses were characterized by multi-angle spectral ellipsometry (J.A. Woollam RC2). The complex refractive index of pPFHDA and p4VP coatings was resolved from ellipsometry data collected at the full wavelength range from 210 nm to 1690 nm and seven different incident angles (45º, 50º, 55º, 60º, 65º, 70º, 75º) from a single-polymer monolayer film (~200 nm) coated on a Si wafer; the multi-angle experiment was to improve the reliability and accuracy of the result. The thickness of p4VP/pPFHDA two-layer on TPU was collected at the 70º incident angle with focus probes (J.A. Woollam) to minimize backside reflections of the transparent TPU. The thickness of each layer was resolved with the known complex refractive index spectra pre-collected on the single-polymer monolayer film, and the wavelength range 400 nm to 1400 nm was used to calculate film thickness using a Cauchy model to avoid modeling complexities associated with absorption and interference from residual backside reflection.

Surface topography characterizations

White-light interferometry profilometer (Zygo, NewView 600) was used to examine the surface topography of the coatings. TPU membranes were fixed on a stainless-steel ring embedded with an O-ring on its bottom. The side with coating was denoted as the front side. The backside of the membrane was pressurized pneumatically by a custom-built 'bulging' device to deflect the membrane and generate strain. The membrane deflection was measured by a laser profiler (Keyence, LJ-X8080), and the pressure was recorded by a pressure gauge (Dwyer DPGAB-04). An equibiaxial strain of the pneumatically deformed membrane can be calculated using the following **Equation (1)**:

$$\varepsilon = \frac{\sqrt{A}-\sqrt{A_0}}{\sqrt{A_0}} = \frac{\sqrt{2\pi r\hbar}-\sqrt{\pi a_0^2}}{\sqrt{\pi a_0^2}} \quad (1)$$

where A is the membrane area in the deformed state and A_0 is the membrane area in the undeformed state (A_0= 46.57 cm^2).

The a_0 is the radius of the membrane in the undeformed state (a_0= 3.85 cm). Assuming a geometrical relation for a spherical cap, valid for a small strain, one can calculate A from the radius of curvature, r, and the measured deflection, h. It should be noted that r can be calculated using h and a_0, as shown in **Equation (2)**:

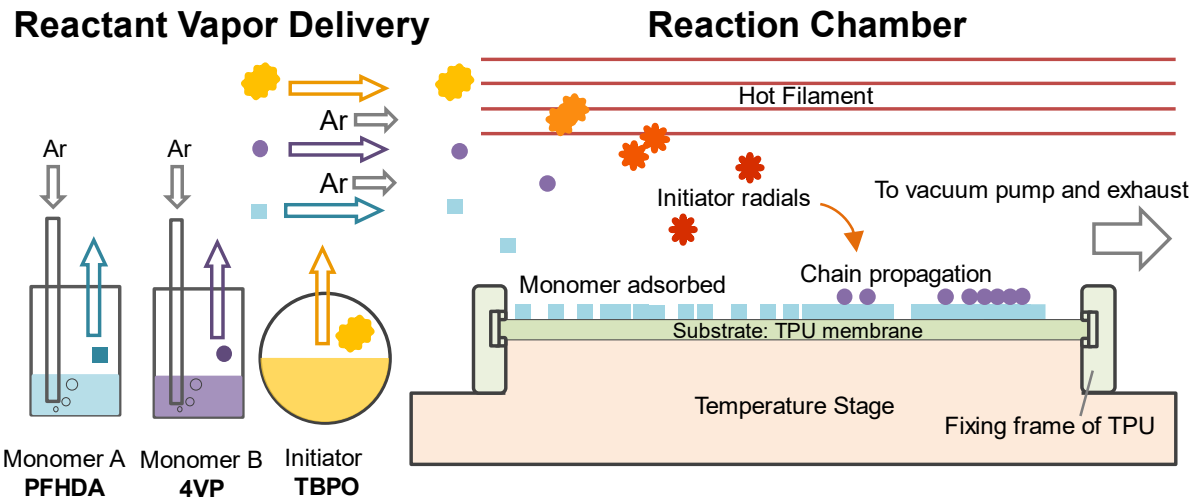

Figure 1 Cartoon depiction of the iCVD deposition system and process.

$$r = \frac{a_0^2 + h^2}{2h} \quad (2)$$

For in situ monitoring of the surface topography of the coating, the TPU and the 'bulging' device were placed under the objective lens of the Zygo profilometer. The strain was then generated pneumatically and determined by the pressure reading which had been calibrated against the deflection previously in the laser profiler. The profilometer was focused on the surface of the TPU at each targeted strain individually after the pressure was stabilized and the vibration was dissipated. The same area of 400×300 μm was imaged as the strain progressing. Filmetrics ProfilmOnline platform was used to process the imaged data. The images were flattened using forth-order fitting and artificial interference patterns caused by persistent vibrations were also removed. No smoothing algorithm was used to preserve the original surface information. Bare TPU was also imaged using Zeiss optical microscope.

Optical properties

The reflectance of the TPU was measured by reflectometry (Filmetrics F-20 UV) at the normal incident angle. The same TPU was measured before and after the AR coating. The reflection from the front (coating) side and the uncoated backside were both included in the reflectance spectrum. The reflectometer is properly baselined before each measurement using a standard Si wafer placed at the same distance as the TPU membrane from the probe to ensure a consistent intensity. The transmittance of the coated and uncoated TPU was measured by a spectrometer (PerkinElmer Lambda 900) in transmission mode.

Simulation

The reflectance simulation of TPU substrate coated with different multi-layer polymer ARCs was conducted by CompleteEASE ellipsometry software from J.A. Woollam (version: 6.61). All reflectance data are at the normal incident angle. The optical constants of TPU for the simulation were collected by ellipsometer at 45°, 50°, 55°, 60°, 65°, and 70° incident angles (reflection), and transmission mode. A pPFDA (1H,1H,2H,2H-perfluorodecyl acrylate) film was deposited on a Si wafer and its spectrum of the complex refractive index was precisely obtained by ellipsometry. The deposition parameters of pPFDA are available at the end of the supplementary information. The optical constants of pPFHDA, pPFDA, p4VP, and TPU were used as input variables for the simulation.

Results and Discussions

Preparation of the two-layer polymer ARC by iCVD

The two-layer polymer antireflection coating (ARC) was prepared by a custom-built iCVD system depicted in Figure 1. A layer of p4VP and a second layer of pPFHDA were sequentially deposited onto a soft TPU substrate of which the structure is shown in Figure 2a. The monomers, 4-vinylpyridine (4VP) and 1H,1H,6H,6H-perfluorohexyl diacrylate (PFHDA), were separately introduced into the vacuum chamber using a bubbler system, which injects argon through a dispersion tube into liquid monomer carrying the vapor into the reaction chamber. This forced vapor delivery enables deposition of monomers with extremely low volatility, which are otherwise infeasible in conventional iCVD relying on vapor pressure for flow.[52] The initiator, di-tert-butyl peroxide (TBPO), was introduced as vapor (without carrier gas) and decomposed by the hot filament to form gas-phase radicals. The two-step initiation process is complete after the radicals encounter adsorbed monomers on the substrate. Gas phase reactions of the radicals are insignificant due to the low chamber pressure of 750 mTorr, ensuring heterogeneous polymerization on the surface and

conformal coatings with controllable chemical compositions.[46, 57, 58] The substrate was placed on a temperature stage to keep the temperature constant and stable, usually around room temperature (35°C).

Fourier-transform infrared spectroscopy (FTIR) was used to characterize the chemical composition of the coating. The spectra of the two-layer polymer coating on TPU, pPFHDA homopolymer, p4VP homopolymer, and bare TPU from 1800

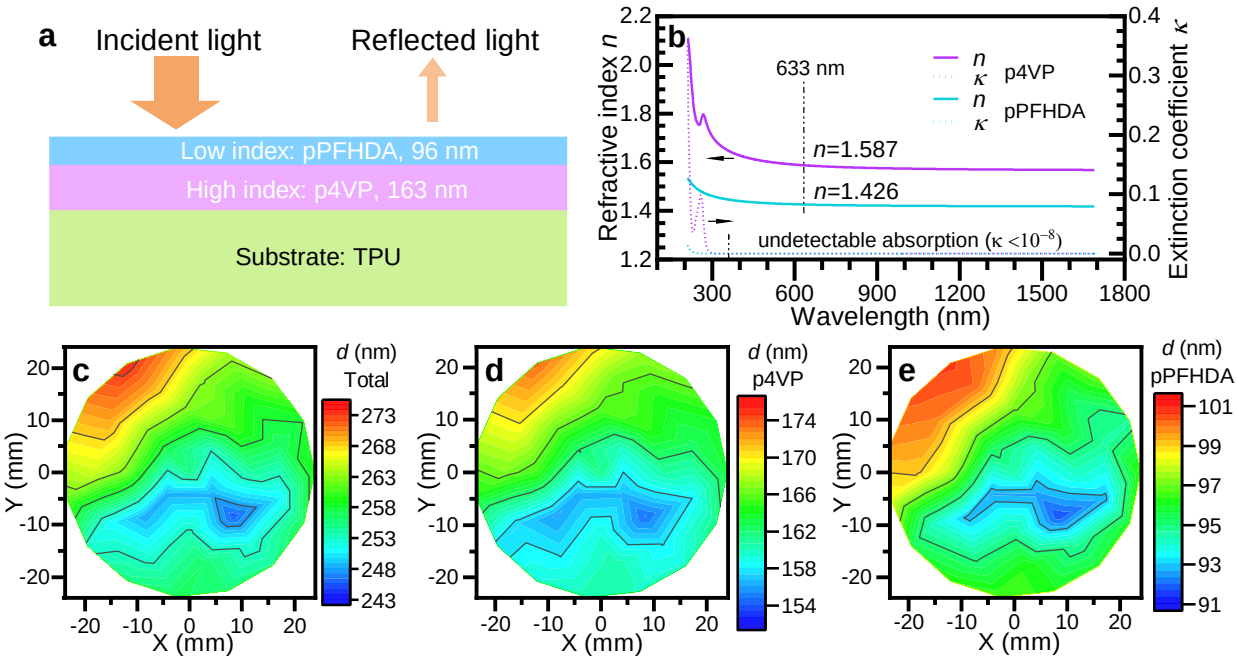

Figure 2 (a) Structure of the two-layer ARC on TPU, and (b) optical constants of individual polymer layers in the design: p4VP and pPFHDA. Contour map of the thicknesses of the (c) two-layer ARC, (d) p4VP layer, and (e) pPFHDA layer on TPU. The mapped area is 18 cm².

The complex refractive index of p4VP and pPFHDA were characterized by ellipsometry and plotted in Figure 2b. The refractive indexes of p4VP and pPFHDA are 1.59 and 1.43 at 633 nm, respectively. The imaginary component of the refractive index, the extinction coefficient, shows both polymers have negligible absorption ($\kappa<10^{-8}$) from near-UV (360 nm) to near-IR (1690 nm)–essential for optical transparency. The total thickness of the two-layer system and the individual films were mapped over the TPU substrate using ellipsometry - see Figures 2c to 2e. The total thickness of the two-layer ARC is 258 nm with ±7.0 nm standard deviation. The thickness of p4VP and pPFHDA are 163 ±4.8 nm and 96 ±2.4 nm, respectively – evidence of good uniformity of iCVD films. Judging by the similar thickness distribution in both layers, the areal thickness variation is likely induced by a local temperature difference due to imperfect contact between the TPU membrane substrate and the temperature stage coupled with the low thermal conductivity of the TPU substrate. In iCVD, the deposition rate is highly correlated to substrate temperature, which governs the adsorption of monomers to the surface; low temperatures result in a larger monomer concentration and a higher deposition rate.[46, 57-59] The uniformity was similar to that achieved in our previous study of a single-layer pPFHDA. [52] Therefore, high uniformity was preserved for multilayer coatings by iCVD, which is a prerequisite for meaningful thickness control and optical coating fabrication.

Chemical structure analysis

cm^{-1} to 700 cm^{-1} (the "fingerprint" region of the spectra) are shown in Figure 3. The full spectra over the entire mid-infrared range are available in Figure S1. The strong stretching mode of the pyridine ring at 1598 cm^{-1} is observed in both the p4VP

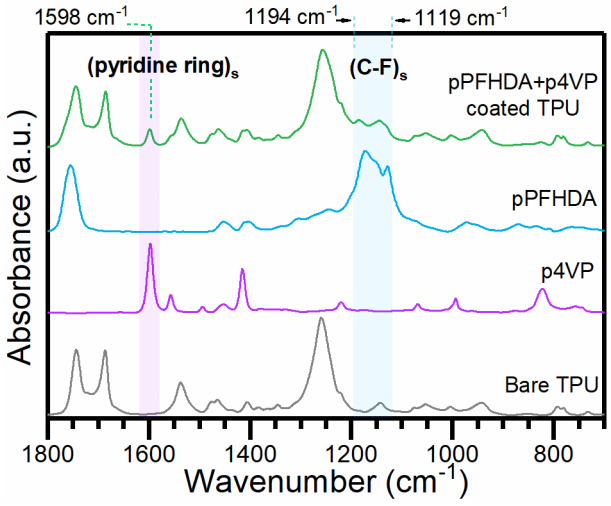

Figure 3 FTIR-ATR spectra of the two-layer polymer coating on TPU, pPFHDA homopolymer, p4VP homopolymer, and bare TPU substrate at fingerprint region from 1800 cm^{-1} to 700 cm^{-1}. Homopolymers spectra were acquired from iCVD films deposited on Si wafers separately.

homopolymer and the coated TPU but not in the other spectra. Also, in Figure S2, aromatic C-H stretch modes of the pyridine ring in p4VP are observed in the coating, indicating that p4VP

was successfully incorporated into the coating. It is important to note that the evanescent wave from the diamond prism of the ATR has a penetration depth of approximately 1 μm–much larger than the coating thickness. Thus, the spectrum of the two-layer coating is dominated by the TPU vibrational modes. Despite the pPFHDA layer being less than 100 nm thin, the strong symmetric and asymmetric C-F stretching modes of -CF_2- observed in the pPFHDA homopolymer are also present in the coated TPU–no other vibrational modes from bare TPU or p4VP in this wavelength range. This indicates the existence of pPFHDA in the coating of TPU. In addition, a comparison of IR spectra between the monomers and the coated homopolymers on a Si wafer is shown in Figure S3. The C=C stretching mode at 1637 cm^{-1} in PFHDA (medium intensity) and the =C-H out-of-plane deformation band of the vinyl group at 927 cm^{-1} in 4VP (strong intensity), are completely absent in the polymer coatings, indicating that the monomers have been fully polymerized and few residual vinyl groups remain.[60] Hence, it can be concluded that the two-layer coating of pPFHDA and p4VP coating has been successfully prepared on the TPU substrate by iCVD.

In situ coating surface topography with progressing strain: polymers vs inorganics

To assess the fracture resistance of the polymer ARC and its superiority over inorganic coatings for flexible optics, an *in-situ* characterization method was designed to compare their fracture behavior with applied strain. Progressive equibiaxial strain was generated stepwise using an established approach (experimental configuration shown in Figure S4), where pressure was applied pneumatically to the coated TPU sample.[61, 62] The cell was placed under a white-light interference profilometer so the surface topography evolution of the coatings could be monitored *in situ*. Profilometry images were collected at strains of ε=0.30%, ε=0.84%, and ε=1.64%, which were calculated by Equation (1) using previous pressure-deflection calibration measured with a laser profiler. A larger strain was not attempted as the corresponding deflection exceeded the maximum measurable by the laser profiler. Initially, comparisons were made between the polymer ARC and films of MgF_2, a conventional inorganic ARC material used as a control sample. MgF_2 films (thickness mapping by ellipsometry shown in Figures S5a and b) were deposited onto the TPU substrates by electron-beam evaporation. Figure 4a to 4c reveals how the surface topography of the polymer ARC evolved–no sign of any cracks was observed even after it was strained to an aggressive value of 1.64%. It is worth noting that flexible optics such as electrically tunable lenses usually involve an applied strain much less than 1%, which is usually limited by the voltage requirement by an electrostriction mechanism.[63, 64] The polymer ARC can readily accommodate these strains. The profilometry images before and after the strain were also presented in Figures S6a and b, and the areal roughness analyzed from them was kept unchanged at 2.7 nm (mean

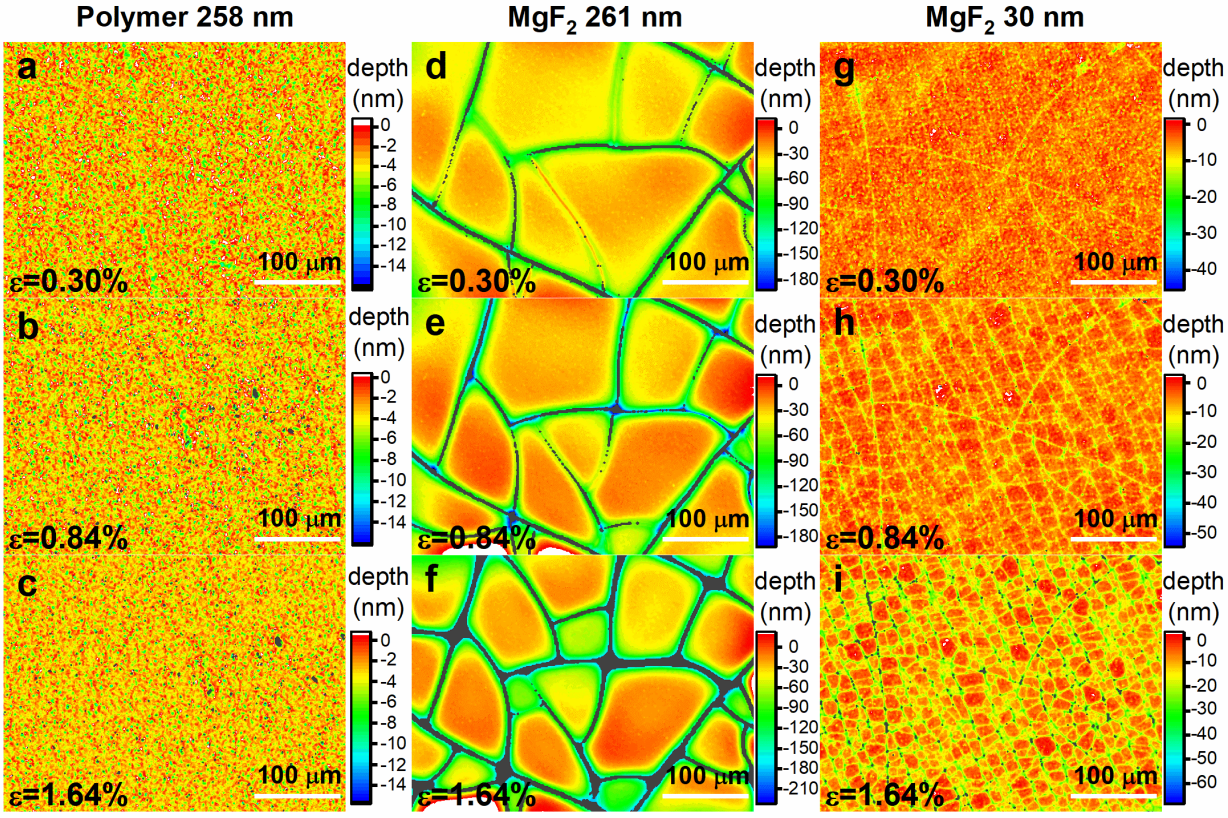

Figure 4 The surface topography of the (a-c) two-layer polymer ARC, (d-f) 261 nm MgF2, and (g-i) 30 nm MgF2 film measured in situ as a function of increasing equibiaxial strain of (a, d, g) ε=0.3%, (b, e, h) ε=0.84%, and (c, f, i) ε=1.64%. The scanned area was 400×300 μm.

square root height). This indicates a very smooth surface was obtained, which is crucial to minimize light loss from scattering.

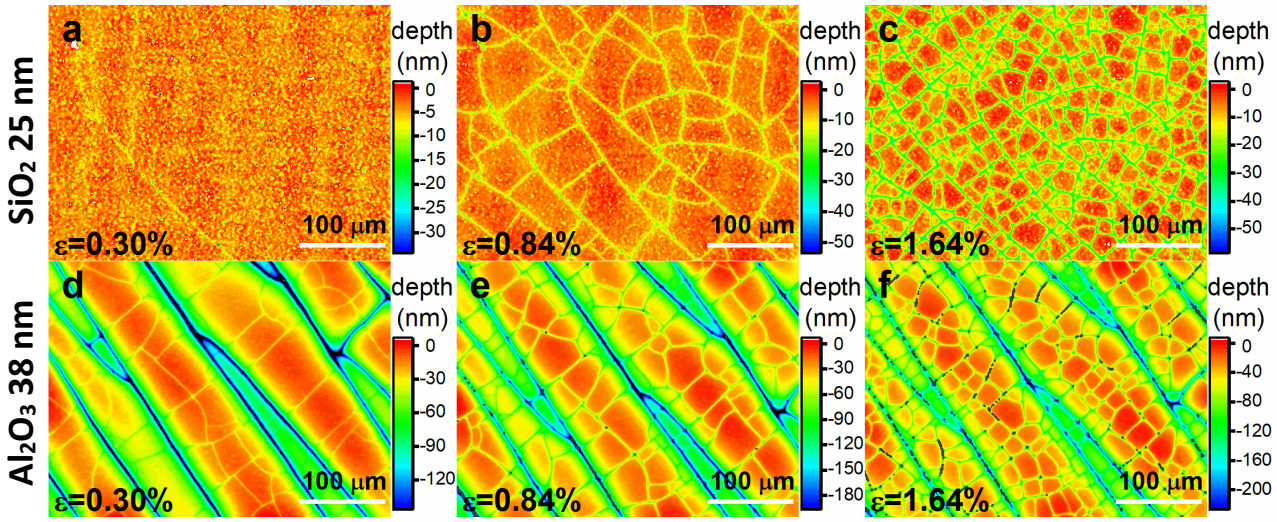

Figure 5 The surface topography of the (a-c) 25 nm SiO_2 coating and (d-f) 38 nm Al_2O_3 coating on TPU were monitored with increasing equibiaxial strain (a, d) ε=0.3%, (b, e) ε=0.84%, and (c, f) ε=1.64%. The scanned area was 400×300 μm.

In contrast, the MgF_2 coating at a comparable thickness (261 nm) fractured into several fragments, resulting in the commonly observed "mud-cracking" phenomenon.[61] This was consistent with our expectations and previously reported studies of the behavior of a brittle inorganic coating on a flexible substrate under strain.[61, 62, 65] Even at the lowest applied strain (ε=0.3%, Figure 4d), the MgF_2 had clearly fractured. As the strain increased, new cracks were initiated (see Figures 4d to 4f); the MgF_2 coating fractured into smaller fragments and the width of the cracks also expanded. In fact, cracks could be observed even before any strain was applied externally (Figure S7), likely due to a large mismatch in elastic properties and/or thermal expansivity between the hard MgF_2 coating and the soft TPU polymer substrate;[66-69] a slight change in temperature and/or humidity in the environment can induce significant internal stress.[20, 70] Because film internal stress is proportional to film thickness, a much thinner (30 nm) film of MgF_2 was deposited onto TPU for fracture characterization to make the experiment more stringent.[65] The 30-nm thickness was also closer to the lower limit of layer thicknesses applied in real multilayer antireflection designs.[26] As expected, Figure 4g reveals fewer cracks in the 30 nm MgF_2 films at low strain (ε=0.3%) relative to the 261 nm-MgF_2 coating; the width of each crack is also appeared to be thinner. According to Andersons and Leterrier, the cracks at this initial stage have large spacing, which is consistent with our observation, and they primarily reflect the defect distribution in the coating.[62] However, when the strain increased to ε=0.84% (Figure 4h), a large number of cracks formed instantaneously, and the coating was fragmented into numerous small pieces. This could indicate the stress transferred from the polymer substrate reaches the strength of the coating so it fragmentated until the size of individual piece was reduced to below a critical value where the stress exerted upon it no longer exceeded its strength.[62] Further increasing the strain to ε=1.64% (Figure 4i) lead to an expansion of crack width as observed in the thicker coating. Therefore, it is safe to conclude that MgF_2 coatings, regardless of thickness, are likely to fracture, even at a small strain of 0.3%, and do not remain intact on flexible substrates.

To further investigate the generality of coating fracture on this TPU substrate, two additional inorganic coatings were prepared using common conventional optical coating materials–SiO_2 and Al_2O_3. They were both deposited onto soft TPU substrates by e-beam evaporations at a carefully controlled deposition rate (<0.5 Å/s) to achieve good film quality and uniformity. Ellipsometry mapping of the film thicknesses on TPU and refractive indexes on a monitor Si substrate (coated at the same time as TPU) are provided in Figures S8 and S9. The thickness of these two inorganic coatings was intentionally designed to be thin (around 30 nm) to reduce internal stress and vulnerability to fracture. As thicker films are likely to fracture at lower strains this is essentially a "best case" scenario for these coatings. Figures 5a to 5c present the evolution of the surface topography of the 25 nm-SiO_2 coating on TPU. Consistent with the behavior of the 30-nm MgF_2, at a small strain (ε=0.3%), only a few cracks were found in localized areas due to defect-induced fracture. The major area of the coating remained intact. However, as the strain increased to 0.84%, the coating fragmented. With the strain further increasing to 1.64%, large pieces further broke into smaller units, as was observed in MgF_2 coating.

Figure 5d to 5f display the surface morphology of the 38 nm-Al_2O_3 coated sample with increasing strain. Interestingly, the alumina-coated TPU possessed a wrinkled morphology. The characteristic periodicity of these wrinkles was several hundred micrometers, and the depth of the "valleys" was in the range of several hundreds of nanometers–much larger than the 38-nm Al_2O_3 coating. This morphology is attributed to residual coating stresses due to thermal effects during evaporation. Alumina required a higher e-beam current for evaporation, which resulted in a more severe radiative heating of the substrate than in SiO_2 or MgF_2 depositions. Though the exact temperature of the substrate was not available, the TPU frame was warm to the touch upon removal from the chamber; this was not the case

after coating the other materials. This temperature excursion during deposition resulted in thermal expansion of the TPU, which then contracts upon cooling to room temperature, resulting in residual stress on the hard alumina film and attendant wrinkling of the substrate.[71-73] This is a well-established phenomenon that has been exploited to characterize mechanical properties of thin film coatings.[74-76] It also further emphasizes the challenges associated with residual film stresses due to mismatches of coefficients of thermal expansion. [18] Thus, the ability of iCVD to coat materials at near-ambient temperatures is an important feature of the deposition method. Even with the wrinkled morphology, the fracture behavior of alumina thin films with applied equibiaxial strain can still be observed. Alumina revealed the same behavior as the other inorganic materials–fracturing into multiple smaller fragments with increasing strain.

To further challenge the durability of the two-layer polymer ARC, the surface topography of the film was characterized after applying repeated strains of the TPU. After aggressively strained 80 times to ε=1.64%, the strained surface was imaged in situ (Figure 6a). Some small cracks can be observed, which were absent initially (Figure 4c); they only appeared after repeated strain cycling. Interestingly, the cracks appeared to emanate from pinhole-like defects. These 'pinhole' defects were widely observed on the pristine uncoated TPU membranes, as shown in Figure S10. Thus, it is possible that the polymer coating was imperfect and discontinuous at these point defects, which combined with stress concentration upon application of strain, led to crack initiation. Moreover, the cracks appeared to only radiate from the defect points for a limited length without intercepting each other. The majority of the film remained intact with no sign of fragmentation. These could indicate the stress transferred to the film surface had not exceeded its strength at this strain due to the elasticity of the polymer coating. Besides the short propagation length (~30 μm) of the cracks, their width and depth detected by the profilometer were small as well. A depth profile across the surface along the indication line is presented in Figure 6b. It shows that the width of a crack is in the range of <10 μm and extends ~15 nm deep– or below the detectable limit of the equipment as the interferometry could not detect the entire depth of these narrow cracks. Still, the fracture behaviors of the polymer coating were distinct from that of inorganics under the same strain state regardless of thickness. The 250 nm-MgF_2 coated sample strained to ε=1.64% was again compared to the polymer film morphology; the corresponding images are provided in Figure 6d. It was obvious that the cracks on MgF_2 were much longer, wider, and deeper than those on polymer film, and the coating, as well as other inorganic coatings, were fragmented into isolated pieces. In contrast, the iCVD polymer coating remained in one piece. The depth profile of 250 nm-MgF_2 coating at the same strained state (ε=1.64%) as the polymer is also shown in Figure 6e. In contrast to that of the polymer, the profile of MgF_2 shows a crack of about 50 μm wide and at least 150 nm deep. These results illustrate that not only are polymer films more resistant to cracking under equibiaxial strain, but even when cracks do form with repeated application of extreme strain, only small cracks form that do not span the entire coating and most of the film remains intact. Starting with substrates possessing higher surface quality and fewer 'pinhole'-like defects, even higher resistance to strain fatigue of the polymer coating may be achieved.

In addition, an intriguing 'crack closure' behavior of the polymer coating was observed. Figure 6c and 6f showed the surface of both the polymer coating and the MgF_2 coating after being released from the high strain state (ε=1.64%) to a lower strain (ε=0.3%). Surprisingly, the cracks in the polymer film appeared to fully close at this state of strain; they essentially disappeared and could not be resolved in the profilometer. An image of the coating after the strain was fully released (ε=0%) is also presented in Figure S11 and shows no sign of cracks as well. The cracks in MgF_2, however, did not fully close and the

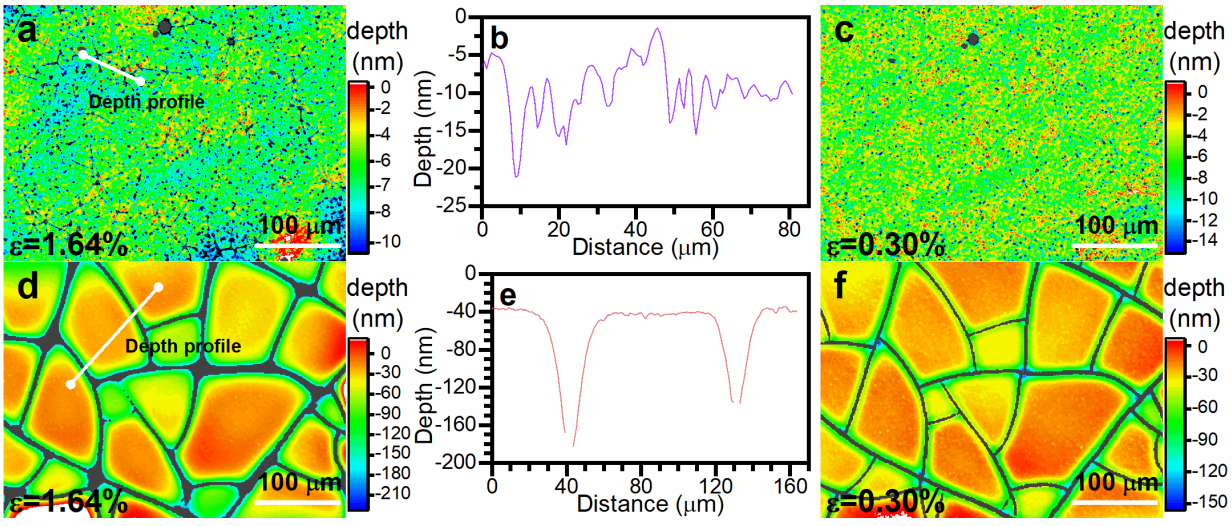

Figure 6 Polymer two-layer ARC (258 nm) imaged after repeatedly strained to ε=1.64% 80 times (a) at ε=1.64% and (c) after strain released to ε=0.3% of the same area; 261 nm-MgF2 imaged during the first strain (d) at ε=1.64% and (f) after strain released to ε=0.3%; Depth profile cross cracks on (b) the polymer ARC surface and (e) the MgF_2 along the indicated lines shown in the images on their left.

shattered fragments did not reconsolidate into a uniform, isotropic film. The cracks remained even after the release of strain but with a narrowed yet substantial width. The depth profile along the same line after the strain was reduced to 0.3% is shown in Figure S12 where the crack was still at least 60 nm deep. The other two inorganic coatings, SiO_2 and Al_2O_3, demonstrated a similar behavior (shown in Figure S13a and b, respectively) despite being thinner. Due to the flexibility of polymer films, these polymeric ARCs can be considered "self-healing". Such behavior has been observed and reported before.[77] In optical applications, this would be a desirable property as large cracks can scatter light and compromise optical performance. The "self-healing" crack closure allows polymer coating to maintain its optical design, such as antireflection, even after aggressive abuse conditions.

Antireflection effect

The reflectance of the TPU membrane with and without the two-layer polymer ARC is presented in Figure 7a. The reflectance spectra include reflection from both the front surface which was coated by iCVD and the uncoated backside. The refractive index of the TPU is 1.51 at 633 nm, and its dispersion spectrum can be found in Figure S14. The calculated reflectance spectra of the bare TPU and coated TPU, with backside reflection (only considering primary backside reflection) are presented in Figure S15, which was in good agreement with the experimental measurement. After the two-layer polymer ARC was applied to the front side of the TPU, the reflectance of visible light from 400 nm to 750 nm was reduced significantly from 7.8% to about 5.86% (including backside reflection). Correspondingly, the reduced reflectance excluding the backside reflection of the TPU with ARC was calculated and displayed in Figure 8.

The reflectance was monitored after the TPU coated with polymer ARC was aggressively strained (ε=1.64% equibiaxial) repeatedly to generate cracks. The reflectance spectra were reported every 40 times of the strain cycles in Figure 7a, while the evolution of the average reflectance at the visible wavelength range (400 to 750 nm) is plotted in Figure 7b. Stable reflectance was observed even after 200 cycles. The reflectance (still with backside reflection) recorded after 200 strain cycles is 5.73%, with a slight drop of 0.14 percent point from that of the unstrained sample. This is likely due to dust accumulation and maybe some imperfect closure of cracks increasing light scattering.

Figure 7c shows the measured total transmittance of the TPU sample with and without the two-layer polymer ARC. The uncoated TPU had a transmission of 91.81% in the visible range. The loss of the transmittance was due to a combination of absorption, reflection, and scattering. With the coating, the transmittance increased to 93.23% over the visible range. The increase of 1.42 percentage points was due to the reflection reduction due to the polymer antireflection coating. The improvement in transmission was smaller than what would be expected from the reflection reduction (1.9%). It is worth noting that the transmittance of the coated TPU was measured after the sample was repeatedly strained 200 times and then left unprotected in an indoor environment for one year. Accumulation of dust and contaminant would cause scattering which caused additional transmittance loss. Nonetheless, the stable reflectance or lack of significant degradation/distortion of the reflectance spectra was corroborated by the improved transmittance. The improvement persists even after exposure to environment for one year, which further confirmed the durability of a two-layer polymer antireflection coating on flexible optical devices that undergoes aggressive, cyclic strain.

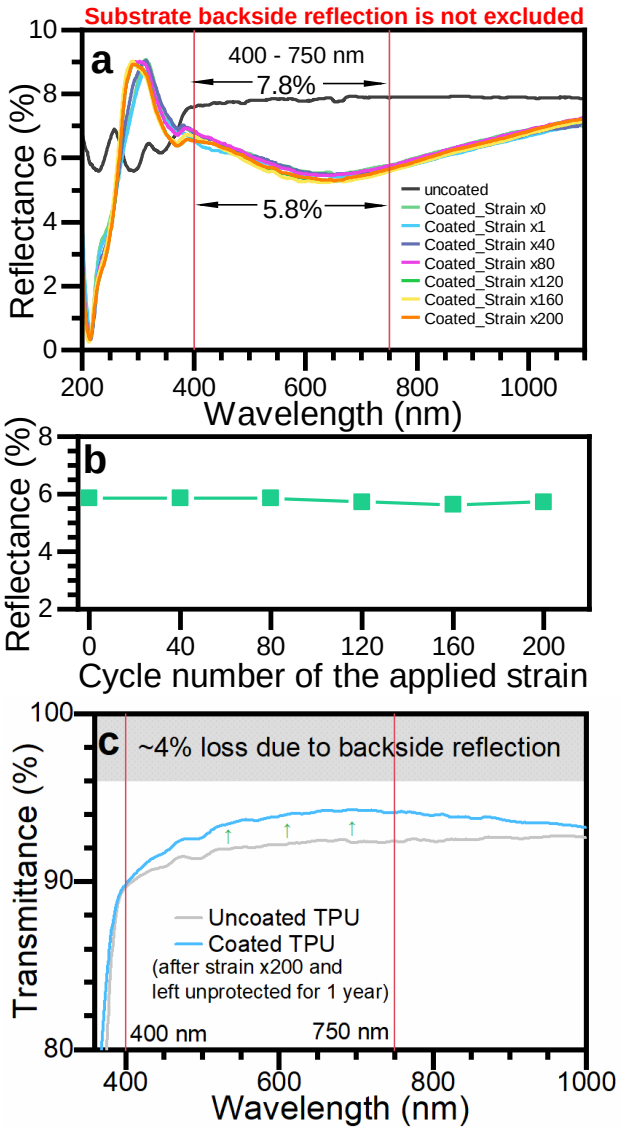

Figure 7 (a) Reflectance spectra of the TPU coated with polymer ARC before and after repeated equibiaxial strain compared to that of uncoated TPU. (b) The reflectance evolution of the ARC-coated TPU at the visible range (400–750 nm wavelength) during repeated strain cycles. The backside (uncoated) reflection of the TPU is included in the measurement. (c) The total transmittance of the bare TPU and polymer ARC-coated TPU after 200 strain (ε = 1.64%) cycles and then stored unprotected for one year.

The polymer ARC studied in this project consisted of only two layers; it is a model system designed primarily to understand the compatibility of polymeric ARCs with flexible, elastomeric substrates and to demonstrate the key processing advantages of iCVD. Thus, the antireflection performance achieved in this study is not fully optimized, and superior performance (lower reflectance) can be

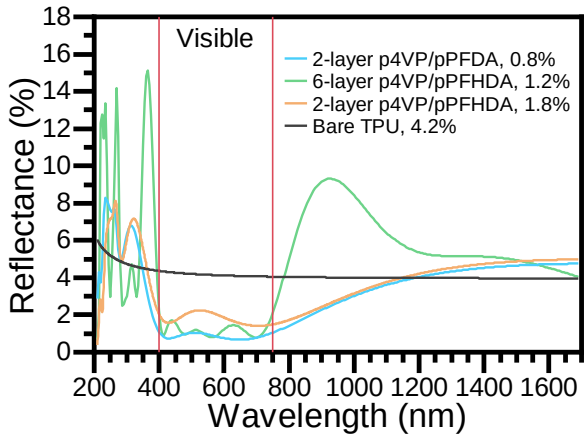

Figure 8 Simulated reflectance of TPU coated with ARC constructed by 6 layers of alternating p4VP/pPFHDA films, 2 layers of p4VP/pPFDA films, 2 layers of p4VP/pPFHDA as deposited in this work, and the bare TPU as reference. Backside reflection (BSR) is not included in the calculation. Average reflectance over visible range is shown in the legend.

achieved with optimized multilayer architectures and alternative polymer thin film compositions. To further explore the potential of polymer ARCs, the effect of additional layers in the multilayer design and greater index contrast was simulated. Unlike solvent-based coating methods, multiple polymer layers can be readily deposited atop previous layers by iCVD without concerns over swelling or dissolution of the coatings, and the precise thickness of each layer can be realized using in situ ellipsometry for example. The layered structure of each optical design is detailed in Table S1. A 6-layer ARC by the same polymers (p4VP and pPFHDA) with an alternating structure reduces the TPU reflectance to 1.17%, of which the spectrum was shown in Figure 8. The calculated reflectance spectrum of the two-layer ARC constructed in this work with backside reflection excluded is also displayed in the plot as a reference. On the other hand, there are polymers with refractive indexes lower than pPFHDA reportedly to be deposited by iCVD, such as poly(1H,1H,2H,2H-perfluorodecyl acrylate) (pPFDA). It has a refractive index of ~1.37 at 633 nm. Substituting pPFHDA in the two-layer ARC with pPFDA alone without adding layers is able to reduce the reflectance to 0.8% (shown in Figure 8). With a simple polymer two-layer ARC, about 80% of the reflection at the visible range can be eliminated and can be enhanced even further with more layers.

Conclusions

Compliant and elastic optical-quality polymer thin films were shown to enable multilayer antireflection coatings (ARCs) that can accommodate deformation strain in flexible optical elements. A two-layer polymeric ARC was deposited by iCVD for the first time. The solvent-free nature of iCVD is critical as it allows the fabrication of complex multilayer designs with high thickness precision while avoiding processing challenges and residual stresses associated with conventional solution processing. Moreover, the polymer ARC design did not require complex surface texturing or patterning. In contrast to conventional inorganic optical layer materials (MgF_2, SiO_2, and Al_2O_3), film fracture was not observed as the polymer ARC deformed up to an extreme equibiaxial strain of 1.64%. Through mechanical cycling of the optical element to this extreme over 200 cycles, minute film fracture was observed, which originated at point defects in the underlying TPU substrate. But as the strain was released, the cracks underwent “crack closure” and became undetectable by optical interference profilometry. This contrasted with inorganic coatings, where large cracks remained after the relaxation of substrate deflection. Finally, simulations of relatively simple ARC designs with established iCVD polymer chemistries showed that broadband reflection of typical optical substrates (n_{633}~1.51) can be reduced from 4% to <0.8% over the visible wavelength range. Through the development of polymer compositions with even greater index contrast and the optimization of multilayer designs, this reflection can be further reduced. With the ability to readily tune composition-structure-property relationships in polymers, iCVD-enabled multilayer ARCs are a compelling alternative to conventional optical coating designs for next-generation flexible optics and optoelectronics.

Author Contributions

The manuscript was written by Yineng Zhao and Wyatt Tenhaeff. Topography characterizations and reflectance measurements over strain cycles were conducted by Ni Huo and Yineng Zhao. Other experiments and analyses were conducted by Yineng Zhao. Sheng Ye conceptualized the product, outlined the mechanical measurement methods, and supplied uncoated TPU samples. All authors have approved the final version of the manuscript. Yineng Zhao and Ni Huo contributed equal effort to this work.

Conflicts of interest

The authors declare funding support from Meta and patent pending.

Acknowledgements

The authors thank Meta Reality Labs for financially supporting the research project. This work was also supported by the National Science Foundation under Grant No. CBET-1827904 (ellipsometer) and CBET-1845805 (FTIR). The authors appreciate the assistance on cleanroom and PVD provided by James Mitchell. The authors also thank Mr. Michael Pomerantz and Dr. Jim Elman for helping with profilometry. The authors particularly thank Kenneth Marshall for helping with the transmission measurement.

References

1. H. K. Raut, V. A. Ganesh, A. S. Nair and S. Ramakrishna, *Energy & Environmental Science*, 2011, **4**, 3779-3804.
2. Z. Han, Z. Jiao, S. Niu and L. Ren, *Progress in Materials Science*, 2019, **103**, 1-68.

3. N. Shanmugam, R. Pugazhendhi, R. Madurai Elavarasan, P. Kasiviswanathan and N. Das, *Energies*, 2020, **13**.
4. M. Moayedfar and M. K. Assadi, *Reviews on Advanced Materials Science*, 2018, **53**, 187-205.
5. H.-W. Yun, G.-M. Choi, H. K. Woo, S. J. Oh and S.-H. Hong, *Current Applied Physics*, 2020, **20**, 1163-1170.
6. G. Tan, J.-H. Lee, Y.-H. Lan, M.-K. Wei, L.-H. Peng, I.-C. Cheng and S.-T. Wu, *Optica*, 2017, **4**, 678-683.
7. Z. Zhao, B. K. Tay and G. Yu, *Appl Opt*, 2004, **43**, 1281-1285.
8. C. Martinet, V. Paillard, A. Gagnaire and J. Joseph, *Journal of Non-Crystalline Solids*, 1997, **216**, 77-82.
9. B. Richards, *Solar Energy Materials and Solar Cells*, 2003, **79**, 369-390.
10. X. Sun, X. Xu, J. Tu, P. Yan, G. Song, L. Zhang and W. Zhang, 2019.
11. H. Chatham, *Surface and Coatings Technology*, 1996, **78**, 1-9.
12. K. L. Jarvis and P. J. Evans, *Thin Solid Films*, 2017, **624**, 111-135.
13. P. C. With, U. Helmstedt and L. Prager, *Frontiers in Materials*, 2020, **7**, 13.
14. K. Pfeiffer, L. Ghazaryan, U. Schulz and A. Szeghalmi, *ACS Appl Mater Interfaces*, 2019, **11**, 21887-21894.
15. G. John, S. R. Jadhav, V. M. Menon and V. T. John, *Angew Chem Int Ed Engl*, 2012, **51**, 1760-1762.
16. S. Cai, Z. Han, F. Wang, K. Zheng, Y. Cao, Y. Ma and X. Feng, *Science China Information Sciences*, 2018, **61**, 060410.
17. S. R. Forrest, *Nature*, 2004, **428**, 911-918.
18. J. A. Rogers, T. Someya and Y. Huang, *Science*, 2010, **327**, 1603.
19. H. Li, Y. Cao, Z. Wang and X. Feng, *Opt. Mater. Express*, 2019, **9**, 4023-4049.
20. W. Vellinga, J. T. M. De Hosson and P. Bouten, *Journal of Applied Physics*, 2012, **112**, 083520.
21. J. Hora, C. Hall, D. Evans and E. Charrault, *Advanced Engineering Materials*, 2018, **20**, 1700868.
22. U. Schulz and N. Kaiser, *Progress in Surface Science*, 2006, **81**, 387-401.
23. J. W. Gooch, in *Encyclopedic Dictionary of Polymers*, ed. J. W. Gooch, Springer New York, New York, NY, 2011, DOI: 10.1007/978-1-4419-6247-8_9716, ch. Chapter 9716, pp. 605-605.
24. R. R. Reddy, Y. Nazeer Ahammed, K. Rama Gopal and D. V. Raghuram, *Optical Materials*, 1998, **10**, 95-100.
25. E. K. Macdonald and M. P. Shaver, *Polymer International*, 2015, **64**, 6-14.
26. A. Musset and A. Thelen, in *Progress in Optics*, Elsevier, 1970, vol. 8, pp. 201-237.
27. H. Jiang, W. E. Johnson, J. T. Grant, K. Eyink, E. M. Johnson, D. W. Tomlin and T. J. Bunning, *Chemistry of Materials*, 2002, **15**, 340-347.
28. D. Langhe and M. Ponting, *Manufacturing and novel applications of multilayer polymer films*, William Andrew, 2016.
29. J. Bailey and J. S. Sharp, *Journal of Polymer Science Part B: Polymer Physics*, 2011, **49**, 732-739.
30. T. Komikado, S. Yoshida and S. Umegaki, *Applied Physics Letters*, 2006, **89**, 061123.
31. T. Komikado, A. Inoue, K. Masuda, T. Ando and S. Umegaki, *Thin Solid Films*, 2007, **515**, 3887-3892.
32. A. L. Álvarez, J. Tito, M. B. Vaello, P. Velásquez, R. Mallavia, M. M. Sánchez-López and S. Fernández de Ávila, *Thin Solid Films*, 2003, **433**, 277-280.
33. J. Bailey and J. S. Sharp, *Eur Phys J E Soft Matter*, 2010, **33**, 41-49.
34. M. F. Weber, C. A. Stover, L. R. Gilbert, T. J. Nevitt and A. J. Ouderkirk, *Science*, 2000, **287**, 2451-2456.
35. K. D. Singer, T. Kazmierczak, J. Lott, H. Song, Y. Wu, J. Andrews, E. Baer, A. Hiltner and C. Weder, *Opt. Express*, 2008, **16**, 10358-10363.
36. M. Li, W. Liu, F. Zhang, X. Zhang, A. A. A. Omer, Z. Zhang, Y. Liu and S. Zhao, *Solar Energy Materials and Solar Cells*, 2021, **229**, 111103.
37. W. Schrenk and T. Alfrey Jr, *Polymer blends*, 1978, 129-165.
38. S. Hansen and T. Robitaille, *Applied physics letters*, 1988, **52**, 81-83.
39. D. B. Chrisey, A. Piqué, R. A. McGill, J. S. Horwitz, B. R. Ringeisen, D. M. Bubb and P. K. Wu, *Chem Rev*, 2003, **103**, 553-576.
40. D. M. Mattox, *Handbook of physical vapor deposition (PVD) processing*, William Andrew, 2010.
41. H. Usui, 2009.
42. H. Usui, *Functional Polymer Films: 2 Volume Set*, 2011, 287-318.
43. B. Wang, C. J. Ruud, J. S. Price, H. Kim and N. C. Giebink, *Nano Lett*, 2019, **19**, 787-792.
44. B. Wang, J. S. Price and N. C. Giebink, *Optica*, 2017, **4**, 239-242.
45. P. Sundberg and M. Karppinen, *Beilstein J Nanotechnol*, 2014, **5**, 1104-1136.
46. K. K. Gleason, *CVD polymers: fabrication of organic surfaces and devices*, John Wiley & Sons, 2015.
47. X. Li, X. Yu and Y. Han, *J. Mater. Chem. C*, 2013, **1**, 2266-2285.
48. Z. Wang, H. Ding, D. Liu, C. Xu, B. Li, S. Niu, J. Li, L. Liu, J. Zhao, J. Zhang, Z. Mu, Z. Han and L. Ren, *ACS Appl Mater Interfaces*, 2021, **13**, 23103-23112.
49. S.-I. Bae, Y. Lee, Y.-H. Seo and K.-H. Jeong, *Nanoscale*, 2019, **11**, 856-861.
50. U. Schulz, *Appl Opt*, 2006, **45**, 1608-1618.
51. Z. Wu, J. Walish, A. Nolte, L. Zhai, R. E. Cohen and M. F. Rubner, *Advanced Materials*, 2006, **18**, 2699-2702.
52. Y. Zhao, N. Huo, S. Ye, A. Boromand, A. J. Ouderkirk and W. E. Tenhaeff, *Advanced Optical Materials*, 2021, **9**, 2100334.
53. S. J. Yu, K. Pak, M. J. Kwak, M. Joo, B. J. Kim, M. S. Oh, J. Baek, H. Park, G. Choi and D. H. Kim, *Advanced Engineering Materials*, 2018, **20**, 1700622.
54. A. M. Coclite, R. M. Howden, D. C. Borrelli, C. D. Petruczok, R. Yang, J. L. Yagüe, A. Ugur, N. Chen, S. Lee and W. J. Jo, *Advanced Materials*, 2013, **25**, 5392-5423.
55. M. O. Mavukkandy, S. A. McBride, D. M. Warsinger, N. Dizge, S. W. Hasan and H. A. Arafat, *Journal of Membrane Science*, 2020, **610**, 118258.
56. C. D. Petruczok, R. Yang and K. K. Gleason, *Macromolecules*, 2013, **46**, 1832-1840.
57. K. K. Lau and K. K. Gleason, *Macromolecules*, 2006, **39**, 3688-3694.
58. K. K. Lau and K. K. Gleason, *Macromolecules*, 2006, **39**, 3695-3703.
59. W. E. Tenhaeff and K. K. Gleason, *Advanced Functional Materials*, 2008, **18**, 979-992.

60. G. Socrates, *Infrared and Raman characteristic group frequencies: tables and charts*, John Wiley & Sons, 2004.
61. Y. Leterrier, D. Pellaton, D. Mendels, R. Glauser, J. Andersons and J.-A. Månson, *Journal of Materials Science*, 2001, **36**, 2213-2225.
62. J. Andersons, Y. Leterrier and I. Fescenko, *Thin Solid Films*, 2003, **434**, 203-215.
63. L. Chen, M. Ghilardi, J. J. C. Busfield and F. Carpi, *Front Robot AI*, 2021, **8**, 678046.
64. F. Xia, Z.-Y. Cheng, H. S. Xu, H. F. Li, Q. M. Zhang, G. J. Kavarnos, R. Y. Ting, G. Abdul-Sadek and K. D. Belfield, *Advanced Materials*, 2002, **14**, 1574-1577.
65. Y. Leterrier, *Progress in Materials Science*, 2003, **48**, 1-55.
66. K. V. K. Rao, S. V. N. Naidu and P. L. N. Setty, *Acta Crystallographica*, 1962, **15**, 528-530.
67. R. A. Orwoll, in *Physical properties of polymers handbook*, Springer, 2007, pp. 93-101.
68. D. Bailey, F. Calderwood, J. Greiner, O. Hunter Jr, J. Smith and R. Schiltz Jr, *Journal of the American Ceramic Society*, 1975, **58**, 489-492.
69. H. J. Qi and M. C. Boyce, *Mechanics of Materials*, 2005, **37**, 817-839.
70. K. Kim, H. Luo, A. K. Singh, T. Zhu, S. Graham and O. N. Pierron, *ACS Appl Mater Interfaces*, 2016, **8**, 27169-27178.
71. N. Bowden, S. Brittain, A. G. Evans, J. W. Hutchinson and G. M. Whitesides, *nature*, 1998, **393**, 146-149.
72. S. Yu, X. Zhang, X. Xiao, H. Zhou and M. Chen, *Soft Matter*, 2015, **11**, 2203-2212.
73. T.-X. Gao, Y.-D. Sun, Y.-F. Feng and S.-J. Yu, *Philosophical Magazine*, 2016, **96**, 2943-2952.
74. J. Genzer and J. Groenewold, *Soft Matter*, 2006, **2**, 310-323.
75. J. Y. Chung, T. Q. Chastek, M. J. Fasolka, H. W. Ro and C. M. Stafford, *ACS Nano*, 2009, **3**, 844-852.
76. Y. Li, B. Fang, J. Zhang and J. Song, *Thin Solid Films*, 2012, **520**, 2077-2079.
77. Y. Zhang, R. Yang, S. M. George and Y.-C. Lee, *Thin Solid Films*, 2011, **520**, 251-257.